Two-photon decay in gold atoms

R. W. Dunford, E. P. Kanter, B. Krässig, S. H. Southworth, and L. Young
Argonne National Laboratory, Argonne, Illinois 60439, USA

P. H. Mokler
Inst. f. Atom-Molekülphysik, Justus-Liebig University, D35392 Giessen, Germany and GSI, Planckstrasse 1, D64291 Darmstadt, Germany

Th. Stöhlker
GSI, Planckstrasse 1, D64291 Darmstadt, Germany

S. Cheng
Department of Physics, University of Toledo, Toledo, Ohio 43606, USA
(Received 18 April 2006; published 13 July 2006)

We have measured the energy differential transition probabilities for the two-photon decay of K vacancies in gold atoms (nuclear charge $Z=79$). This is the heaviest atom for which this information has been obtained, and so is most sensitive to relativistic effects. The experiment determined the shape of the continuum radiation for the transitions $2s \rightarrow 1s$, $3s \rightarrow 1s$, $3d \rightarrow 1s$, and $(4s+4d) \rightarrow 1s$ at an emission pair opening angle $\theta = \pi/2$. Our results for $3d \rightarrow 1s$ and $(4s+4d) \rightarrow 1s$ extend to energies above and below the region of the intermediate state resonances. No relativistic calculations exist for Au, so we compare with calculations by Mu and Crasemann and Tong *et al.* for Ag ($Z=47$) and Xe ($Z=54$). For equal-energy, back-to-back two-photon decay, the calculations show an increase in transition probability with Z for the $2s \rightarrow 1s$ and $3d \rightarrow 1s$ transitions. In contrast, our data, at $Z=79$, corrected for the angular distribution, give a smaller transition probability than the lower-Z experimental results of Ilakovac *et al.* and Mokler *et al.* for Ag and Xe. The shapes of the two-photon continua in our data are in general agreement with theory except that we find anomalously high values for the differential two-photon transition probability for the $3s \rightarrow 1s$ transition near $y=0.35$, where y is the fraction of the transition energy carried by the lower-energy photon.

DOI: 10.1103/PhysRevA.74.012504 PACS number(s): 31.30.Jv, 32.80.Wr, 32.30.Rj

I. INTRODUCTION

An inner-shell vacancy in a neutral atom decays predominantly either by emission of a single photon or an Auger electron. But it can also decay by the simultaneous emission of two photons. The two-photon decay mode proceeds via a complete set of virtual intermediate states and therefore provides a unique means of studying the complete structure of the atom. Two-photon decay was first proposed by Maria Göppert-Mayer in 1929 [1,2] in the early days of the quantum theory, and she predicted that this would be the primary decay mode of the $2^2S_{1/2}$ level of hydrogen where selection rules forbid all single-photon transitions to the $1^2S_{1/2}$ ground state in the nonrelativistic limit. The initial experimental interest was in the field of astrophysics [3,4] where two-photon decay was found to contribute to the continuum radiation from planetary nebulae [4]. The main interest at the present time is in comparisons between theoretical calculations and laboratory experiments in heavy atoms and ions where many-electron effects, relativistic effects, and strong field strengths prevail and thus provide a challenge to theory. A recent review of the theoretical and experimental work on two-photon decay is given in Ref. [5]. Here we report a measurement of the differential decay probability for two-photon decay of K vacancies in gold atoms ($Z=79$).

A. Theoretical

In the nonrelativistic limit, the rate for the emission of two electric dipole photons ($2E1$) by a hydrogenlike atom with one of the photons having a frequency between ν_1 and $\nu_1 + d\nu_1$ has the form [6]

$$w(\nu_1)d\nu_1 = \frac{2^{10}\pi^6 e^4}{h^2 c^6}\nu_1^3\nu_2^3 |M_{fi}|^2_{\mathrm{av}} d\nu_1. \tag{1}$$

The matrix element M_{fi} for the transition must be averaged over the directions of propagation and polarization for each of the two photons. It is given by

$$M_{fi} = \sum_n \left(\frac{(\hat{\varepsilon}_1 \cdot \vec{r})_{fn}(\hat{\varepsilon}_2 \cdot \vec{r})_{ni}}{\nu_{ni} + \nu_2} + \frac{(\hat{\varepsilon}_2 \cdot \vec{r})_{fn}(\hat{\varepsilon}_1 \cdot \vec{r})_{ni}}{\nu_{ni} + \nu_1} \right), \tag{2}$$

where $\hat{\varepsilon}_i$ are the polarization vectors for photon 1 and 2, the index n refers to intermediate p states, $\nu_{ni} = \nu_n - \nu_i$, $(\hat{\varepsilon}_k \cdot \vec{r})_{ij}$ are electric dipole matrix elements, and the sum is over all discrete and continuum states. The photons emitted in this process form a continuum, but the sum of the energies of the two coincident photons from each decay is equal to the transition energy. The total two-photon decay rate is given by:

$$w_T = \frac{1}{2}\int_0^{\nu_0} w(\nu_1)d\nu_1, \tag{3}$$

where ν_0 is the transition energy. The factor $\frac{1}{2}$ comes because photon 1 is counted twice in the interval $\{0,\nu_0\}$.

The nonrelativistic result for the $2E1$ decay of the $2^2S_{1/2}$ state in hydrogenlike atoms, after averaging over photon polarizations, is given by [7,8]

$$\frac{d^3w}{dE_1 d\Omega_1 d\Omega_2} = \frac{Z^4\alpha^6 2^5}{(2\pi)^3 3^8}(1+\cos^2\theta)y(1-y)\phi^2(y), \tag{4}$$

where θ is the opening angle between the two photons, and y is the fraction of the transition energy $E_0 = E_1 + E_2$ carried by one of the photons. The factor $y(1-y)\phi^2(y)$ describes the shape of the distribution and is independent of the nuclear charge Z. The shape is found to be a broad continuum with a maximum at half the transition energy which gradually drops to zero at the end points. All of the Z dependence of the differential transition probability is contained in the overall scaling factor Z^4. The total decay rate is obtained by integration over energy and photon emission angles and has an overall Z^6 dependence since the energy integration contributes another factor of Z^2. The opening angle θ between the two photons in the lowest-order theory has a $(1+\cos^2\theta)$ distribution.

For two-photon decay of inner-shell vacancies in many-electron atoms, the dominant mode is $2E1$ and so the initial and final states must have the same parity [9]. The most important cases are for decay of a K hole with an electron undergoing transitions $ns \rightarrow 1s$ and $nd \rightarrow 1s$. Although fully relativistic calculations for inner-shell two-photon decay have been done for only a few special cases, nonrelativistic calculations and extensive theoretical work in H-like and He-like ions [5] provide guidance for estimating the transition rates, Z dependence, angular distributions, and spectral shapes for these processes. Freund was the first to suggest that two-photon transitions between inner-shell vacancy states could be observable [10]. Following this, a number of theoretical studies, both nonrelativistic [11–14] and relativistic [15,16], have been reported. Nonrelativistic self-consistent-field calculations for Mo have been done by Bannett and Freund [13,17] and for Ar, Kr, Xe, and Rn by Wu and Li [12]. These calculations were done in the electric-dipole approximation. Relativistic self-consistent-field calculations have been done for Mo, Ag, and Xe by Tong, Li, Kissel, and Pratt [15] and by Mu and Crasemann [16,18]. These calculations include higher-multipole transitions beyond $2E1$, and the summations over intermediate states include all bound (occupied and unoccupied) and continuum states.

An early theoretical question about the theory of two-photon decay in neutral atoms was concerned with whether to include the occupied bound states of the atom in the sum over intermediate states. Guo [19] proved that the Pauli exclusion principle does not prohibit summing over all intermediate states including occupied bound states. If such occupied states lie between the initial and final states (e.g., the $2p$ state in the two-photon transition $3d \rightarrow 1s$), then there is a large increase in the differential transition probability ("intermediate-state resonance") when the energies of the photons approach the values of a cascade decay via these levels. This is the same phenomenon studied for hydrogen-like systems by Tung *et al.* [20], and Florescu [21].

The intermediate state resonances are already included in the formulas for two-photon transitions [e.g., Eq. (1)]. If one of the denominators in Eq. (2) vanishes at a given photon frequency, that one term will dominate the expression near that frequency. The usual procedure is to include the width of the state Γ by making the replacement $\nu_n \rightarrow \nu_n - i\Gamma_n/2$ in those terms capable of resonance. Then there is a smooth transition in photon frequency between the two-photon transition regime, where all the intermediate states are virtual, to the cascade regime, where one of the intermediate states resonates. This means that the meaning of the term "two-photon branching ratio" is not well defined except for $2s \rightarrow 1s$ transitions. Drake [22] and Savukov and Johnson [23] address this issue. Drake uses a definition of the total two-photon decay in which one integrates the second-order formula (with its sum over a complete set of states) from $E = 0$ to $E = E_0$ including all resonances, and then subtracts an individual squared term for each resonance.

B. Experimental background

Two-photon decay from inner-shell-vacancy states of many-electron atoms was first seen by Bannett and Freund [13,17] by measuring photon coincidences between two solid-state (Si-Li) x-ray detectors. Inner-shell vacancies were produced by irradiating a thin Mo foil with Ag x rays from a sealed x-ray tube. They observed both $2s \rightarrow 1s$ and $3d \rightarrow 1s$ decays in molybdenum. The continuum shape was not well determined as the measurements were made over a restricted energy range near the midpoint of the distribution. Ilakovac *et al.* [24–26] used radioactive sources to generate K vacancies in xenon, silver, and hafnium and studied the two-photon decays of these excited atoms. They used a pair of high-purity germanium detectors and also applied the photon coincidence technique. Two-photon emission in the transitions $2s \rightarrow 1s$, $3s \rightarrow 1s$, $3d \rightarrow 1s$, and $(4s+4d) \rightarrow 1s$ were observed and compared with the various theoretical calculations. They found general agreement with the expected continuum shapes, and, in particular, the single-photon spectra of the $3d \rightarrow 1s$ transitions in silver and hafnium confirmed the predicted intermediate-state resonance effect and supported Guo's assertion about the need to include the occupied levels in the sum over the intermediate states. Schäffer and collaborators [27,28] reported measurements of the two-photon decay branches in Ag induced by nuclear electron capture. The angular dependence of the two-photon emission was also probed by Schäffer and co-workers. For $ns \rightarrow 1s$ transitions, a $1+\cos^2\theta$ distribution is expected and for $nd \rightarrow 1s$ transitions a $13+\cos^2\theta$ distribution is expected [20,29]. Schäffer *et al.* studied both 180° and 90° photon emission in order to confirm the difference in the angular distributions. They found reasonable agreement between experimental results [28] and theoretical values from Tong *et al.* [15].

The goal of the present work in inner-shell two-photon decay is to explore higher-Z atoms where we can study relativistic effects. Relativity modifies the structure of heavy atomic systems and, hence, influences the differential two-photon decay rates. Moreover, higher multipole amplitudes may contribute non-negligibly to two-photon decay in heavy systems. In particular, we are interested in the spectral shapes of the continuum radiation and the opening angle distributions of the photons. Such differential measurements provide a more detailed test of the theoretical calculations. In earlier work at the Advanced Photon Source (APS), we made a preliminary measurement [30,31] of two-photon decay following photoionization of the K shell in Au ($Z=79$). We obtained measurements of transition probabilities for ns or nd electrons to fill the K vacancy. Due to the limited statistical accuracy and high background, the results were restricted to the case in which the two photons had nearly the same energy. In this paper, we describe an improved measurement with lower background and better statistical accuracy in which we have measured the triply differential two-photon decay rate at an opening angle of 90° for an arbitrary energy partition between the two photons. For the more intense $3d \rightarrow 1s$ and $(4s+4d) \rightarrow 1s$ lines, we have been able to measure the transition probability through the region of the cascade resonances $[1s] \rightarrow [2p] \rightarrow [3d]$ and $[1s] \rightarrow [2p] \rightarrow [4d]$ or $[4s]$. Here, $[nl]$ denotes a vacancy in the nl subshell.

II. EXPERIMENT

Inner-shell two-photon decay has to compete with the fast, allowed decay modes of single-photon and Auger emission. The wings of the intense characteristic x-ray lines and backgrounds from x-ray scattering mask the two-photon spectrum. Only coincident detection of the two photons can discriminate against these backgrounds. We chose to study Au atoms in order to compare with a recent measurement of two-photon decay of the 2^1S_0 level in heliumlike Au ions [32] done at the SIS heavy ion accelerator at GSI in Germany. We created K vacancies in a Au target by photoionization with x rays provided by the APS at Argonne National Laboratory. While the use of radioactive sources to produce the inner-shell vacancies in earlier experiments by Ilakovac *et al.* [24–26] and by Mokler *et al.* [28], had advantages in the relatively low background and slow rate of accidental coincidences observed, we used photoionization for our experiment in Au because of the lack of a suitable radioactive source. The photoionization technique also has some further advantages. The intense x-ray beam available from the APS allowed us to use very thin Au targets. This minimized backgrounds from electron and photon scattering in the target material and minimized the correction for self-absorption. Since we had the ability to control the rate of K-hole production to optimize the detection rate, the experiment was completed in two weeks as compared to the many months of counting required for the source experiments. Also, we were able to set the accidental coincidence rate to an acceptable level, and, in the end, the accidental coincidences were not an important factor in determining our statistical accuracy. The major limitation arose, rather, from true coincidences caused by strong cascade transitions. The use of photoionization also avoids the complication caused by the change in charge of the nucleus and the subsequent rearrangement of the atomic shells associated with nuclear electron capture. This effect needs to be considered when a radioactive source is used to create the K vacancy [33].

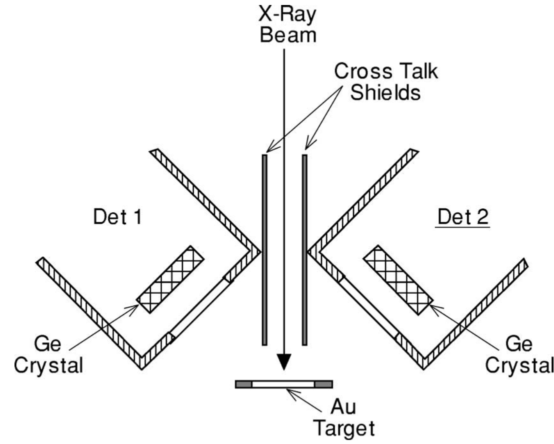

FIG. 1. Schematic diagram of the interaction region. Two germanium solid-state detectors measure two-photon decays with opening angles near 90°. Cross-talk shields prevent coincidences caused by photons scattering between the detectors.

The experimental arrangement in our interaction region is shown in Fig. 1. We used x rays from the wiggler beamline 11-ID-B at the Basic Energy Sciences Synchrotron Radiation Center (BESSRC) at the APS [34]. The beamline monochromator was set to deliver 90.3 keV x rays, well above the Au ionization energy of 80.7 keV. The beam size (about 2×2 mm) was defined by a set of four-jaw slits located in the beamline in front of our hutch. A second set of slits located in the hutch provided "clean-up." The x rays were incident on a 1-mg/cm^2 Au target and passed on to a shielded beam dump located downstream. Two shielded Ge solid-state detectors arranged in the polarization plane of the primary x rays at 135° to the beam direction and 90° to each other measured x rays from the target. Ta shields located between the two detectors suppressed "cross-talk" events. Each of the detectors was surrounded by Pb, and Pb walls were located in front of and behind the target to cut down on background from scattered x rays. Our preliminary run [30] had been done at the Bending Magnet beamline 12BM at the APS. At the wiggler, we enjoyed higher x-ray fluxes and were able to use a thinner target. We also increased the cross-talk shielding between the detectors for this run.

The Ge detectors each had a 0.0127 cm Be window and we added a 0.0127 cm kapton window to the front of each detector to reduce the possible background from electrons coming from the target. The detector preamplifiers provided separate energy and timing signals. The energy signals were shaped with an integration time of 6 μs. The energy resolution of each detector was about 500 eV full width at half-maximum at 88 keV.

Events for which there was a coincidence between the two detectors within 5 μs were recorded on tape. Also 1% of the singles events, in which only one of the two detectors

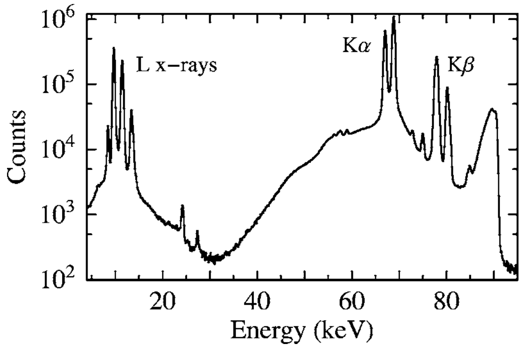

FIG. 2. Log plot of the spectrum recorded in detector 1. The feature near 90 keV is due to Rayleigh and Compton scattering of the incident x-ray beam. The four peaks below 20 keV are Au Lx rays, and the four prominent peaks between 60 and 80 keV are the $K\alpha_2$, $K\alpha_1$, $K\beta_{1,3}$, and $K\beta_2$ x rays, respectively.

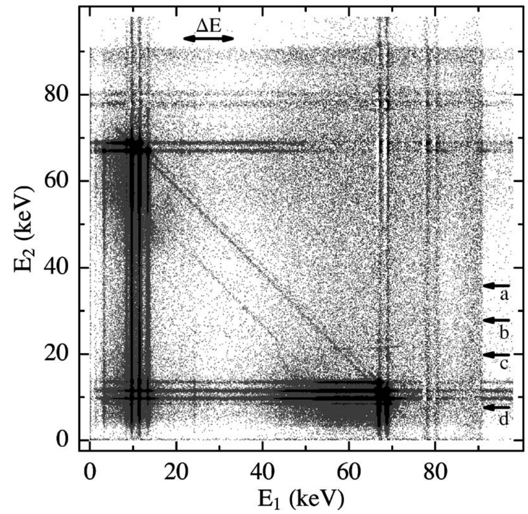

FIG. 3. Coincidence intensity after subtraction of random coincidences. The data are plotted as a function of the energies E_1 and E_2 deposited in detectors 1 and 2 with 90 keV x rays incident on a 1 mg/cm^2 Au target. The contrast was adjusted to emphasize two-photon decays, which appear as diagonal lines near the center of the figure. The double arrow labeled ΔE shows the energy cut for Fig. 4. The arrows on the right indicate the centers of the windows corresponding to panels (a), (b), (c), and (d) of Fig. 5.

recorded a signal, were saved to tape. The latter were used for general diagnostics and to determine the rate of production of K holes. Any events for which a single detector had two timing signals within 36 μs were flagged as "pileup" events and were rejected and an approximate correction included in the data analysis. The detector rates were each about 7 kHz and the coincidence rate was about 100 Hz. The coincidences were mostly "true" coincidences from cascade transitions such as $[1s]\rightarrow[2p]\rightarrow[3d]$.

A typical spectrum in detector 1 is shown in Fig. 2. The broad trapezoidal-like feature between 85 and 90 keV is Rayleigh and Compton scattering of the incident 90 keV x rays in the target. The peaks at about 78 and 80 keV are predominately the Au $K\beta_{1,3}$ and $K\beta_2$ lines. The most intense lines are Au $K\alpha_1$ from $2\,P_{3/2}\rightarrow 1s$ at 68.8 keV and $K\alpha_2$ from $2\,P_{1/2}\rightarrow 1s$ at 67 keV. The four strong lines below 20 keV are the Au L x rays. The continuum radiation between the L and K x rays is caused by various processes, including incomplete charge collection in the detectors, some pileup which is not rejected by the pileup rejection circuit, escape of Ge characteristic x rays, and Compton scattering of photons in the target and in the material surrounding the detectors. These processes are important in our experiment because the continuum radiation from two-photon decay that we are interested in must be extracted from this background.

Energy calibration of the detectors was done before and after the run with a ^{109}Cd radioactive source, and during the run, using the Au L x rays and K x rays from the on-line data. The detector calibration remained stable and we were able to combine all of the data from the two-week run into one set. The detector calibrations determined from a preliminary read of the data tapes were used to generate "pseudo" parameters including calibrated arrays for the energy spectra of detectors 1 and 2 and one for the sum of the energies in detectors 1 and 2 (sum-energy parameter).

The timing channel from each detector was fed into a time-to-amplitude converter (TAC) which measured the time difference between the signals in the detectors. The time spectrum reflects the time structure of the beam stored in the synchrotron. The pattern repeats at the synchrotron period of 3.68 μs. The true coincidences contribute to a "prompt" peak with a width of about 60 ns. We chose a window from the time spectrum symmetric with the prompt peak to gate the prompt coincidence events and a wider one to gate the accidental coincidences. We subtracted the accidental coincidences (times a scale factor to account for the wider window) from the prompt coincidences to get the true coincidence spectra.

In Fig. 3, we show a spectrum of true coincidence events plotted as a function of the energy deposited in detector 1 versus the energy deposited in detector 2. The diagonal lines near the center of the plot are the two-photon decays which have a fixed value for the sum-energy that is equal to the transition energy for the decay. These are clearly distinguishable from the rest of the coincidences in this plot and this points up the power of the coincidence technique for picking out a weak decay branch from the background. Other features in the plot include the cascade coincidence peaks corresponding to successive K and L x-ray emission from the same atom. Tails from incomplete charge collection or pileup form "ridges" that extend parallel to the axes between the peaks. These ridges are largely true coincidences in which one of the two cascade partners deposits its full energy in the first detector while the other contributes to the low-energy tail or is part of a pileup event in the second detector. In regions of the plot where the two-photon "diagonals" encounter a cascade peak or cross one of the ridges, the background relevant to extraction of two-photon events is high. As we will see, this gives rise to gaps in the determination of the energy differential two-photon transition probabilities.

III. DATA ANALYSIS

Figure 4 displays a histogram of the sum-energy for coincidence events with the condition that the lower-energy

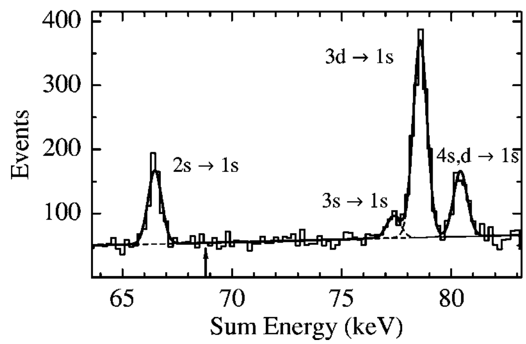

FIG. 4. The histogram is the sum-energy spectrum of coincidences between the two detectors with the condition that the lower-energy photon E_{low} lie between 22 and 33 keV (see double arrow in the upper part of Fig. 3). Random coincidences have been subtracted. The dashed curves show fits to the background and four peaks corresponding to the $2s \rightarrow 1s$, $3s \rightarrow 1s$, $3d \rightarrow 1s$, and $(4s+4d) \rightarrow 1s$, two-photon transitions. The heavy solid line is the sum of the components of the fit. The arrow shows the energy where a $K\alpha_1$ line caused by cross-talk would occur.

photon (E_{low}) of the coincidence pair lies in the range 22–33 keV. These events are from the clean region of Fig. 3 away from the cascade peaks and the horizontal and vertical ridges. Also the random coincidences have been subtracted from this spectrum so these data are true coincidences. The fit to the data was made with a function with four peaks and a linear background using the program gf3 [35]. The peak shape function used by the program is mainly a Gaussian describing complete charge collection of a photon in the crystal, but there is also a skewed Gaussian on the low-energy side which accounts for incomplete charge collection due to effects such as trapping in crystal dislocations. A step function below the peak is also included to account for events arising from escape of photoelectrons from the crystal. We determined the peak shape parameters for each detector (e.g., the relative size of the skewed Gaussian and step function) by fitting x-ray lines from calibration sources and the cascade coincidences from our data and then fixed these parameters for all subsequent fits. The individual fits to the peaks and the background obtained from the program are indicated by dashed lines in Fig. 4. The sum of all of these components is given by the heavy black line. The four peaks correspond to the two-photon transitions $2s \rightarrow 1s$, $3s \rightarrow 1s$, $3d \rightarrow 1s$, and a blend of $4s \rightarrow 1s$ and $4d \rightarrow 1s$.

From preliminary fits to spectra like those of Fig. 4 with wide cuts on E_{low}, we determined a set of widths and positions to be fixed in fits to a set of sum-energy spectra for different values of E_{low}. For each spectrum, the fit determines the number of events Δn due to the two-photon transitions $2s \rightarrow 1s$, $3s \rightarrow 1s$, $3d \rightarrow 1s$, and $(4s+4d) \rightarrow 1s$. Typical sum-energy spectra used in this procedure are shown in Fig. 5. The top three spectra (a), (b), and (c) have a condition that E_{low} lie in a bin of width $\Delta E_{\mathrm{low}}=4$ keV centered at energies 35.7, 27.7, and 19.7 keV, respectively. These are all in the clean region of Fig. 3.

The histogram in Fig. 5(d) is an example where the fitting procedure described above does not work. Here, $E_{\mathrm{low}}=7.5$ keV. This is in the region of high background near the

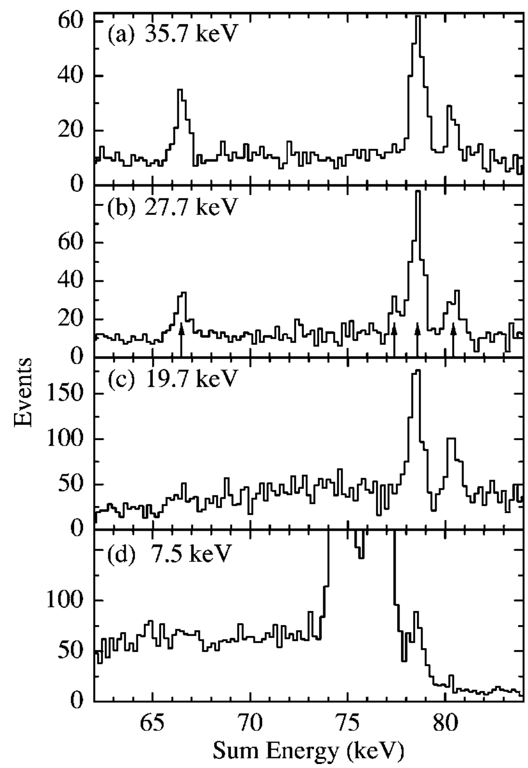

FIG. 5. Sum-energy spectra for coincidences between the two detectors with a condition that the lower energy photon be in a window centered at (a) 35.7 keV, (b) 27.7 keV, (c) 19.7 keV, and (d) 7.5 keV (see arrows in Fig. 3). Random coincidences have been subtracted. The window widths for (a), (b), and (c) are 4 keV, while that for (d) is 0.4 keV. The arrows in (b) show the positions of the $2s \rightarrow 1s$, $3s \rightarrow 1s$, $3d \rightarrow 1s$, and $(4s+4d) \rightarrow 1s$ two-photon transitions.

intense cascade resonance features. Because the energy differential transition probability is changing rapidly here for the two-photon transitions which have resonances, we use a smaller width $\Delta E_{\mathrm{low}}=0.4$ keV. Taking into account that ΔE is an order of magnitude larger for spectrum (b) than for spectrum (d), one can see that the background in Fig. 5(d) in the vicinity of the $2s \rightarrow 1s$ two-photon sum-energy peak is more than 50 times larger than that in Fig. 5(b). This means it is not possible to get any information about the $2s \rightarrow 1s$ energy differential transition probability at this value of E_{low}.

The truncated peaks near a sum energy of 75 keV in Fig. 5(d) arise from the tails of the cascade resonances (more specifically the "ridges" parallel to the axes in Fig. 3) and they mask the region of the $3s \rightarrow 1s$ two-photon resonance. So no information can be obtained about this resonance either. On the other hand, the background on the high-energy side of the truncated peaks is less intense and the $3d \rightarrow 1s$ two-photon resonance is strong enough that it can be seen in Fig. 5(d) as a small but fairly well resolved peak at 78.5 keV. Thus, we can get good information on the differential intensity for the $3d \rightarrow 1s$ two-photon transition at $E_{\mathrm{low}}=7.5$ keV from this spectrum. For the fit to Fig. 5(d), we modify our standard procedure to include the background, the intense resonance peaks (whose shapes are determined by independent preliminary fits), the $3d \rightarrow 1s$ peak, and the $(4s+4d)$

$\rightarrow 1s$ peak. The widths, positions, and shapes of the latter two peaks are fixed at the same values used in the standard fits. A similar procedure is used to obtain fits throughout the "dirty" region near the cascade resonances, i.e., we modify our basic fit to adapt to the features and background present in each particular spectrum, obtaining as much information as possible.

In analyzing the data for the two-photon transitions, we looked for evidence of a systematic effect caused by cross-talk between the detectors. Two processes were of particular concern. The first is a coincidence caused by Compton scattering of a K x-ray photon in one of the detectors followed by detection of the scattered photon in the other detector. The second process involves events in which one of the K x rays is absorbed in one detector but a Ge-K x-ray photon escapes and gives a signal in the second detector. Such events would have a sum energy equal to the energy of one of the K x rays. Some of the sum-energy lines produced in this way would be blended with the sum-energy lines arising from two-photon decay and hence not easily removed in the fitting procedure. These processes were important in the data analysis of Ilakovac [25,26]. See, for example, Fig. 2 of Ref. [26] where blends of $K\alpha_2$, $K\beta_{1,3}$, and $K\beta_2$ are seen. We decided to eliminate these processes using Ta plates between the detectors (see Fig. 1) to prevent all cross-talk. In our preliminary run to measure Au two-photon processes reported in Ref. [30], we also used a Ta shield, and although we did not see K x-ray lines (see Fig. 2 of Ref. [30]), we could not rule them out at the level of accuracy needed for the present work. For this reason, in addition to doubling the thickness of the Ta shields for the second run, we also took extra care in their placement. The main concern was the placement of the Ge crystals relative to the shields, and there was some uncertainty in their positions within the detector cryostats. As a final check, we looked for evidence of the $K\alpha_1$ line at 68.8 keV in our sum-energy spectra (indicated by an arrow in Fig. 4). Such a peak is clearly absent from Fig. 4 and we did not find any evidence of such contamination in any of the other spectra, nor was there evidence of any of the other K x-ray lines in any of our spectra. We concluded that this process did not contribute to the data being reported in this paper. The absence of the K x-ray lines in the sum-energy spectra also rules out a contribution to our data from $np \rightarrow 1s$ two-photon decay.

The differential transition probability P for two-photon decay relative to the total decay rate for a K hole W_K is determined by the formula

$$P = \frac{1}{W_K}\left(\frac{d^3w}{dE d\Omega_1 d\Omega_2}\right) = \frac{\Delta n/\Delta E}{n_K \xi_1 \xi_2 \epsilon_E \Delta\Omega_1 \Delta\Omega_2 B_\ell(\theta)}. \quad (5)$$

Here, n_K is the number of K holes produced in the experiment, and Δn is the number of two-photon events for a given transition in a bin of width ΔE centered at energy E as measured in one of the two detectors. $\Delta\Omega_j$ are the solid angles of the detector crystals subtended at the beam spot on the Au target, ξ_j are the detection efficiencies, $B_\ell(\theta)$ corrects for the opening angle distribution, and ϵ_E is the electronic efficiency [36]. For our experiment, $n_K = 8.7(0.8)\times 10^{10}$, $\Delta\Omega_1 = 0.275(5)$ sr, and $\Delta\Omega_2 = 0.22(1)$ sr.

The angular distribution parameter $B_\ell(\theta)$ ($\ell = s$ for $ns \rightarrow 1s$ and $\ell = d$ for $nd \rightarrow 1s$) corrects for the fact that, although our experiment is designed to measure the differential two-photon transition probabilities at an opening angle $\theta = 90°$, our events are distributed over a range of opening angles because of the finite size of the detectors. Since 90° is a minimum in the opening angle distributions for both $ns \rightarrow 1s$ and $nd \rightarrow 1s$ transitions, this correction factor will be larger than 1. For the $ns \rightarrow 1s$ transitions, we assume a distribution of the form $(1+\cos^2\theta)$, and performing the average over our experimental geometry we find the correction factor $B_s = 1.038(5)$. The error is due to uncertainty in the geometry. For the $nd \rightarrow 1s$ transitions, we assume a distribution of $(13+\cos^2\theta)$, and averaging over the detector faces we find $B_d = 1.0030(5)$. We also considered the correlation between the angular distribution correction and the detector efficiency correction [25], but this was found to be negligible for our experiment.

The detector efficiencies ξ_j vary with photon energy. They account for all factors that enter into the efficiency including the absorption in various materials (Au, air, kapton, Be, Ge dead layer). The ξ_j also account for the escape of Ge x rays and the thickness of the Ge crystal. We determined these efficiencies both using a simple model that accounted for the known energy dependences of absorption, etc., and in independent measurements using calibrated radioactive sources [37]. There was reasonable agreement between the experimental and the modeling methods in the region of overlap (12–100 keV). We chose to correct the data above 12 keV using the experimental measurements supplemented by corrections for the absorbers specific to the experiment. Below 12 keV, we used calculated efficiencies. The uncertainty in the efficiency varies with photon energy being about 10% at the lowest energies measured falling to about 3% at 80 keV.

In order to improve the statistical accuracy for the measurement of the differential transition probabilities, we fit sum-energy spectra for which the low-energy photon of the coincidence pair lies within an energy bin of width ΔE_{low}. This means all events are accounted for in the range of $y = E/E_0$ from $y=0$ to 0.5. This procedure takes advantage of the fact that the energy differential spectra are symmetric about the midpoint $y=0.5$ and effectively folds over the high-energy part of the spectral shape referred to one of the detectors. This also means that the width ΔE that is entered into Eq. (5) is twice the energy cut ΔE_{low}.

The electronic efficiency parameter ϵ_E is energy-dependent but is very close to 1 throughout the range of energies of interest for the two-photon data. The discriminator thresholds were set to accept all energies down to about 2 keV below the lowest-energy L x ray at 8.5 keV. We measured the electronic efficiency at low energy by comparing the relative intensity of the L x rays in each detector (after correcting for the intrinsic detector efficiency) to the expected relative intensities. We found no systematic fall-off in intensity in the region that extends from 14 keV down to 8.5 keV. Below this, we apply an increased error for the two data points for the $3d \rightarrow 1s$ transition and one data point for the $(4s+4d)\rightarrow 1s$ transition that fall in the region between 6.5 and 8.5 keV, where the discriminator threshold is less certain. Another component to the electronic efficiency parameter is the fraction of true coincidence events that fall outside of our cut on the prompt coincidence peak in the TAC spectrum. Since the timing resolution is worse for low-energy photons, this efficiency is energy-dependent. To minimize the losses from counts falling outside the TAC cut, we made the window wide enough that the correction was only a few percent even at the lowest energy for which data were obtained.

Before applying our definition [Eq. (5)] for the relative transition probability P to the data, it is useful to consider how P scales with nuclear charge. If the transition probability for inner-shell two-photon decay scaled in the same way as that for the $2S_{1/2}\rightarrow 1S_{1/2}$ $2E1$ transition in H-like ions, then, using, e.g., Klarsfeld's formula [Eq. (4)], the triply differential transition probability would scale as

$$\frac{d^3w}{dEd\Omega_1 d\Omega_2} \propto Z^4, \tag{6}$$

and since the decay rate for a K hole scales as $W_K \propto Z^4$, the quantity P would be independent of Z. Of course, one would not expect an argument based on simple one-electron atoms to apply rigorously to complicated neutral atoms, but these considerations show that the quantity P is well suited to elucidate the nontrivial changes in atomic structure as a function of nuclear charge, since the trivial part of the Z scaling has been removed.

IV. RESULTS AND DISCUSSION

Figures. 6–8 show our results for P determined from Eq. (5) for the $2s\rightarrow 1s$, $3s\rightarrow 1s$, $3d\rightarrow 1s$, and $(4s+4d)\rightarrow 1s$ two-photon transitions. The error bars are largely statistical and dominated by the uncertainties determined by the fits to the sum-energy spectra, but they also include uncertainties for the parameters n_K, $\Delta\Omega_1$, $\Delta\Omega_2$, ξ_1, ξ_2, ϵ_E, B_ℓ, and the pileup correction, all added in quadrature. Of these, n_K contributes an error of about 10% (due to errors in fitting the singles spectra and uncertainties in the intrinsic detection efficiencies and solid angles), and the rest are less important except for the efficiencies ξ_j and ϵ_E below 8 keV, where they each contribute to the uncertainty at about the 10% level.

Our results for the continuum distribution for the $2s\rightarrow 1s$ transition are shown in Fig. 6(b). As no relativistic calculations exist for inner-shell two-photon decay in Au (Z=79), we compare to existing calculations in Xe (Z=54) and Ag (Z=47). The solid line is a result by Mu and Crasemann [18] for Xe for an opening angle θ=180°, so we have divided their results by 2 in order to compare with our data for θ=90°, assuming an opening angle distribution of $1+\cos^2\theta$. The open diamonds are Mu and Crasemann's result [16] for Ag at an opening angle of 90°, so these results are compared directly to our data. The open boxes are calculations by Tong *et al.* [15] for Ag also for an opening angle of 90° so, again, no correction was required.

There is only a small difference between the Ag and Xe calculations for the $2s\rightarrow 1s$ transitions. This is not surprising

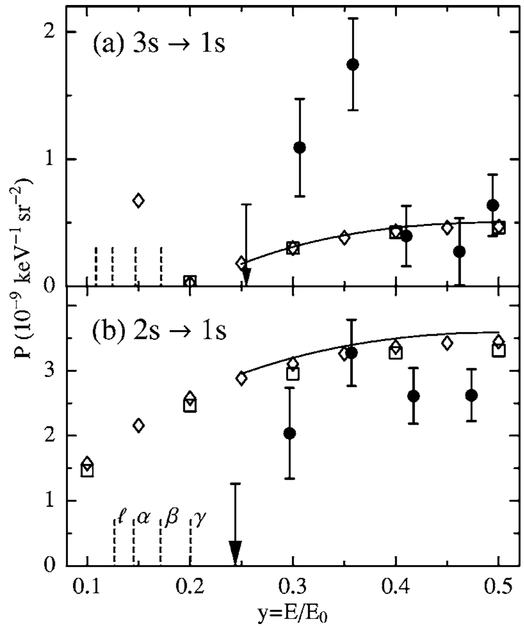

FIG. 6. Solid circles with error bars are the experimental results for the relative differential transition probability P [Eq. (5)] as a function of E/E_0 for (a) $3s\rightarrow 1s$ and (b) $2s\rightarrow 1s$ two-photon decays at 90° opening angle. E is the energy of the lower-energy photon of the coincident pair. The solid lines are the Xe theoretical results of Mu and Crasemann [18] for 180° divided by 2 to correct for angular distribution (see text). The open diamonds are the Ag theory of Mu and Crasemann [16] and the open boxes that of Tong *et al.* [15], both for Ag atoms at 90° opening angle. The dashed lines give the positions of the major L x-ray groups ($L\ell$, $L\alpha$, $L\beta$, $L\gamma$).

in view of our earlier observation that, based on the scaling for H-like ions in the nonrelativistic limit, P would be independent of Z. The calculation of Tong *et al.* for Ag has the same shape as that of Mu and Crasemann but is lower. Our data for Au are generally lower than the calculations, particularly near y=0.24, where only an upper limit on the transition probability P could be obtained. For smaller y, we are in the region of the L x rays (dashed lines) and the background is too high to obtain two-photon transition data for $2s\rightarrow 1s$ [see, e.g., Fig. 5(b)].

Results for the $3s\rightarrow 1s$ two-photon decay are shown in Fig. 6(a). In this case, the Ag calculations by Mu and Crasemann (open diamonds) and Tong *et al.* (open boxes) are in good agreement. Mu and Crasemann's results for Xe (solid line) are in agreement with their Ag results at y=0.3 but slightly higher than their Ag results at y=0.5. The theoretical curves for Ag are nearly zero at y=0.2. This behavior is expected from the theory of hydrogenlike atoms, which predicts a "zero" in the $3s\rightarrow 1s$ emission at y=0.22 [20,29]. The probability P, again, increases toward lower y approaching the cascade resonances at y=0.13 and 0.11 [the two leftmost dashed lines in Fig. 6(a)]. Below y=0.22, the backgrounds in the sum-energy spectra are too high for us to obtain meaningful experimental results for the $3s\rightarrow 1s$ transition.

Above y=0.4 in our data for the $3s\rightarrow 1s$ transition, the errors are too large to discriminate between the different calculations. The errors are even larger in the region y=0.3 $\rightarrow$0.4, where higher than expected transition probabilities

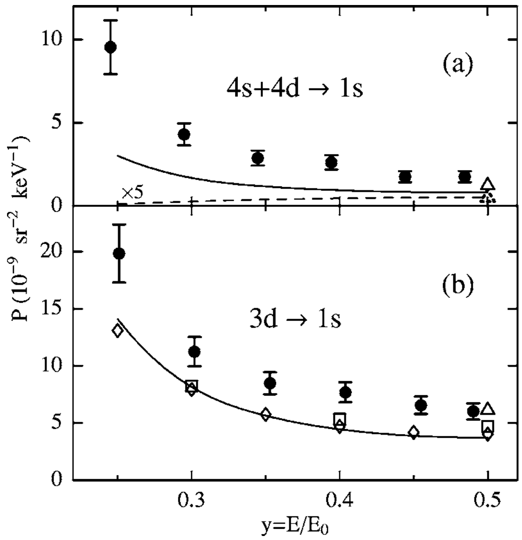

FIG. 7. Solid circles with error bars are the experimental results for the relative differential transition probability P [Eq. (5)] at 90° opening angle as a function of $y=E/E_0$ for (a) the sum of $4s\rightarrow 1s$ and $4d\rightarrow 1s$ two-photon transitions, and (b) $3d\rightarrow 1s$ two-photon transition. E is the energy of the lower-energy photon of the coincident pair. The solid lines in both panels are the theoretical results of Mu and Crasemann [18] and the open triangles at $y=0.5$ are those of Tong *et al.* [15] both for Xe atoms at 180° but corrected here to apply to 90° for comparison to our data (see text). In (a), the dashed line and dashed open triangle (at $y=0.5$) are, respectively, Mu and Crasemann and Tong *et al.*'s results for the Xe $4s\rightarrow 1s$ transition also corrected for to apply to 90° opening angle. The $4s\rightarrow 1s$ calculations have been multiplied by 5 for better visualization. In (b), the open diamonds are the theory of Mu and Crasemann [16] and the open boxes that of Tong *et al.* [15], both for Ag atoms at 90° opening angle.

were measured. This phenomenon can also be seen in the sum-energy spectrum of Fig. 5(b) showing events in a 4-keV-wide cut on E_{low} centered at 27.7 keV ($y=0.36$). There is a prominent peak at the position of the $3s\rightarrow 1s$ transition (77.3 keV, indicated by an arrow). This is in contrast to the sum-energy spectrum of Fig. 5(a), which is events in a 4-keV-wide cut centered at $E_{low}=35.7$ keV ($y=0.46$). Here, there is little evidence of the $3s\rightarrow 1s$ peak. The fitting procedure gives a small positive result as shown in Fig. 6(a) at $y=0.46$ but the error bar for this point is consistent with zero. The anomalously high values of P in Fig. 6 are surprising since, based on theory, P should be near a local maximum at $y=0.46$ and be somewhat lower at $y=0.36$. Because this result is unusual, we checked for other possible sources of systematic errors that might have been missed but did not find any. In particular, many of the potential problems would also affect the close-lying $3d\rightarrow 1s$ resonance or the flat background on the low-energy side of the $3s\rightarrow 1s$ peak, or lead to anomalies in other cuts on the sum-energy spectra. We looked for such effects but did not find any problems. On the other hand, the $3s\rightarrow 1s$ is our weakest line and therefore the most susceptible to statistical fluctuations or unknown experimental problems. Still, the result is interesting and it should be checked in future experimental work.

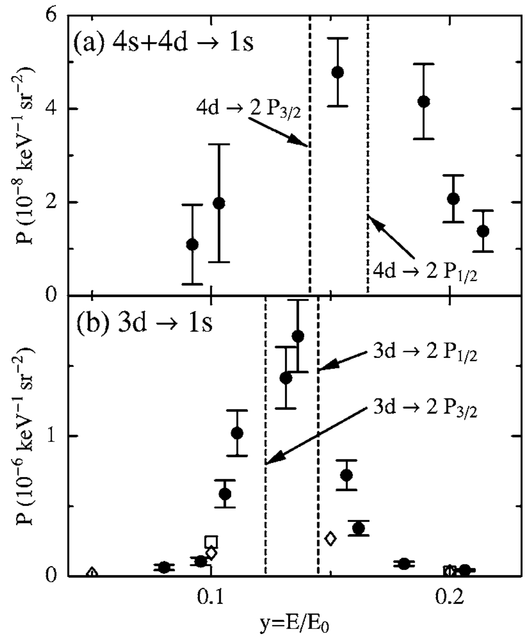

FIG. 8. Solid circles with error bars are the experimental results for the relative differential transition probability P [Eq. (5)] at 90° opening angle as a function of $y=E/E_0$ in the region of the cascade resonances, for (a) the sum of $4s\rightarrow 1s$ and $4d\rightarrow 1s$ two-photon transitions, and (b) the $3d\rightarrow 1s$ two-photon transition. In (b), the open diamonds are the theory of Mu and Crasemann [16] and the open boxes that of Tong *et al.* [15], both for Ag atoms at 90° opening angle. The dashed lines show the positions of the cascade resonances through the $2^2P_{1/2}$ and $2^2P_{3/2}$ levels. Note the different vertical scales.

The differential transition probabilities P for the $3d\rightarrow 1s$ and $(4s+4d)\rightarrow 1s$ two-photon transitions are presented in two parts. Figure 7 shows the experimental and theoretical results for events lying in the clean region of the spectrum of Fig. 3, and Fig. 8 covers the region in the vicinity of the cascade resonances where the transition probabilities are much higher. Figure 7(b) shows the data for $3d\rightarrow 1s$. The solid line is Mu and Crasemann's result for Xe and the open triangle is a calculation by Tong *et al.* These are for an opening angle $\theta=180°$, so we multiplied them by 13/14 to compare to our data for $\theta=90°$ (we assume a distribution $13+\cos^2\theta$). The open diamonds and open boxes are results for Ag at $\theta=90°$ by Mu and Crasemann and by Tong *et al.*, respectively. Mu and Crasemann's results show a slightly different shape for Ag and Xe. Near $y=0.25$, the Ag result lies below the Xe curve while at $y=0.5$ it is above the curve. The calculation by Tong *et al.* for Ag lies above that of Mu and Crasemann's values in this case. It is important to note that both theoretical groups predict that P should increase with Z and our data for Au at 90° are generally higher than the theoretical values for the lower Z atoms. The one exception is Tong *et al.*'s Xe point at $y=0.5$. The data generally follow the continuum shape predicted by theory and, in particular, P is rising rapidly toward lower y. This is a further demonstration of the resonance effect for two-photon transitions that was first confirmed experimentally by Ilakovac and collaborators [26].

Differential transition probabilities for $4s$ and $4d$ two-photon transitions are given in Fig. 7(a). Mu and Crasemann's calculations for Xe corrected to apply to $\theta=90°$ are given by the solid line (sum of $4s\rightarrow 1s$ and $4d\rightarrow 1s$) and the dashed line ($4s\rightarrow 1s$). The results of Tong *et al.* for Xe at $y=0.5$ corrected for $\theta=90°$ are given by the open triangle (sum of $4s\rightarrow 1s$ and $4d\rightarrow 1s$) and the dashed triangle ($4s\rightarrow 1s$). Both theoretical calculations predict that the $4s\rightarrow 1s$ transition contributes only about 10% to the total for $(4s+4d)\rightarrow 1s$ at $y=0.5$ and much less at smaller y (the $4s\rightarrow 1s$ theoretical results are multiplied by 5 in the figure). Consequently, our data largely measure the $4d\rightarrow 1s$ two-photon transition probability. The experimental geometry is unfavorable for measuring the $ns\rightarrow 1s$ transitions due to the suppression from the photon angular distribution, but this is an advantage here, as it helps to effectively isolate the $4d\rightarrow 1s$ transition.

In Fig. 7, the Xe calculation by Tong *et al.* at $y=0.5$ (triangle) is higher than that of Mu and Crasemann (solid line). Again our data qualitatively follow the solid line, but are significantly higher. Here, also, the measurements indicate a significant increase in P for decreasing y, as expected due to the intermediate state resonances.

Since our experiment is sensitive to photons down to about 6 keV, we can explore the two-photon resonance region. These data are given in Fig. 8. Although the background is high, the $nd\rightarrow 1s$ transitions also become more intense near the values of y where they go into resonance, and this allows us to obtain reliable fits in this region. Figure 8(b) gives the $3d\rightarrow 1s$ data (solid circles with error bars). There are two cascade resonances $3d\rightarrow 2P_{1/2}\rightarrow 1s$ and $3d\rightarrow 2P_{3/2}\rightarrow 1s$, and their positions are indicated by the dashed lines. The calculations for Ag by Mu and Crasemann are given as the open diamonds and those for Tong *et al.* are given by the open boxes. All of these are consistent with our results except for the calculation by Mu and Crasemann at 0.15. More extensive calculations that trace out the resonances in detail are needed. If such calculations were available, we could then convolve an experimental resolution function with the calculated values for comparison with our data.

The $(4d+4s)$ resonance region is shown in Fig. 8(a). Again the positions of the resonances are given by the dashed lines. In this case, the two-photon transitions are weaker and so the statistical quality of the data is not as good, but we were able to explore the region on the low-energy side of the resonances as in the case of the $3d\rightarrow 1s$ transitions. There are no relativistic calculations available for the $(4s+4d)\rightarrow 1s$ transition for the region of y displayed here.

In Fig. 9, we show a comparison of the experimental results for $2s\rightarrow 1s$ (a) and $3d\rightarrow 1s$ (b) transitions for the four highest Z atoms where inner-shell two-photon decay has been measured. We also include the theoretical results of Mu and Crasemann (dashed lines) and Tong *et al.* (solid lines). All of these results are for back-to-back, equal-energy photons except for our Au $(Z=79)$ measurements, where the opening angle was 90°. Because of this, we corrected our results using the expected angular correlations so they can be compared to the other data in the plot. The first impression from these two plots is that the experimental results are not changing rapidly with Z. This is expected if the scaling with Z found in the nonrelativistic H-like ions has some relevance here. To the extent there is any variation, the trend in both experimental data sets seems to be a slow drop in transition probability as Z increases. This is in contrast to the theoretical results, which suggest an increase with Z, particularly for $3d\rightarrow 1s$, albeit over a limited range of Z at the left side of the plot. The theoretical results for $2s\rightarrow 1s$ are in good agreement with each other and with the data for Ag and Xe, but the two theoretical results for $3d\rightarrow 1s$ are quite different in magnitude. The calculation of Tong *et al.* is in better agreement with the experimental results for Ag and Xe.

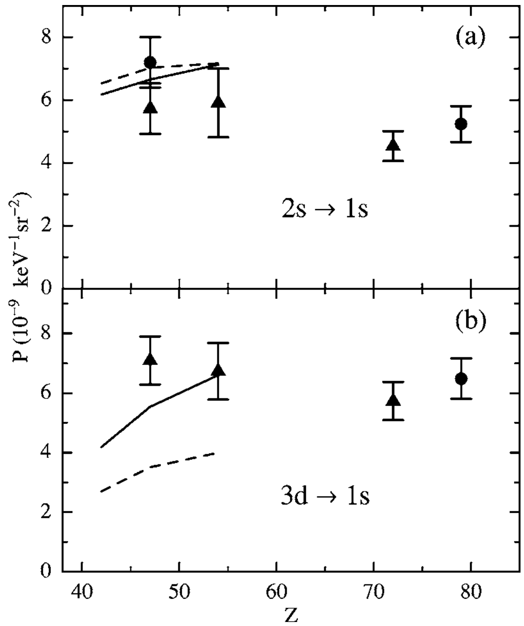

FIG. 9. Theoretical and experimental results for P [Eq. (5)] as a function of the nuclear charge Z. Experimental results for $E_1=E_2$ and $\theta=\pi$ are shown as points with error bars for (a) $2s\rightarrow 1s$ and (b) $3d\rightarrow 1s$. Solid triangles are results by Ilakovac *et al.* [25,26]. The solid circle at $Z=47$ in (a) is the silver result of Mokler *et al.* [28,38]. The solid circles at $Z=79$ are the results of the present experiment. Our data have been extrapolated to 180° [in (a) we multiplied by 2 and in (b) we multiplied by 14/13, as described in the text]. The solid curves show the theoretical calculations by Tong *et al.* [15] and the dashed curves are the theoretical calculations by Mu and Crasemann [16,18] for $E_1=E_2$ and $\theta=\pi$.

V. SUMMARY

This experiment has demonstrated the utility of two-photon transitions in exploring atomic structure, including both energy levels and matrix elements for a complete set of states. Using solid-state x-ray spectrometers, we get differential measurements of the continuum distribution for two-photon transitions. This provides a different perspective on the atomic structure of an atom compared to more conventional measurements of energy levels and lifetimes. Different states contribute to different parts of the two-photon distributions. Near the end points, the low-lying states predominate (sometimes leading to resonant behavior), whereas near the centers of the distributions, more distant levels contribute. Although the transition probabilities are small, the coincidence method provides a powerful means of isolating two-photon transitions. The accuracy is good because one simultaneously measures the strong diagram lines, and these provide a convenient normalization to the data. Our experiment in Au, at relatively high nuclear charge, has allowed exploration of lower relative energies y. The significance of this is that the region of low y is the most sensitive to deviations from the lowest-order calculations [32,39]. The challenge now for the theory of inner-shell two-photon transitions is to address the lower y and resonance regions more completely.

Our data for the continuum distributions P for the $3d \rightarrow 1s$ and $4s+4d \rightarrow 1s$ transitions at $\theta=90°$ opening angle have the same general shape as the theoretical calculations for the lower Z atoms Ag and Xe and, in particular, these curves increase toward lower energy, demonstrating the resonance effect first observed by Ilakovac and collaborators. The data for these transitions generally lie above the theoretical curves. The exception is the calculation by Tong *et al.* for $3d \rightarrow 1s$ at $y=0.5$. The data for $2s \rightarrow 1s$ lie lower than the Ag and Xe calculations and drop more sharply than expected below $y=0.3$. For the $3s \rightarrow 1s$ transition, there is a resonancelike feature near $y=0.35$ that lies well above the theoretical curve.

In general, theory and experiment do not agree as well here as they do for two-photon decay in highly charged ions [39,5]. For the $3d \rightarrow 1s$ transitions, there is disagreement between the available calculations for equal-energy, back-to-back decays (see Fig. 9). In addition, the data for these transition probabilities do not show an increase with Z indicated by theory.

It would be interesting to explore these issues further by measuring two-photon transitions in heavier atoms. Here, also, relativistic effects would be larger and one could explore even lower y, where such effects are expected to contribute more prominently.

The anomaly in the weak $3s \rightarrow 1s$ transition (resonance like feature near $y=0.35$) may be an indication of some omission in the calculations, or it may indicate some as yet not understood systematic effect in our experiment. In either case, it is important to investigate it further with better statistical accuracy, either to help refine the theory or to improve the experiment. In particular, one could check this result in a different atom where, regardless of the cause, the phenomenon will likely look different and the details will give a clue to the cause of this anomaly. In this respect, studying a still higher Z atom would be an advantage because the $3s$ and $3d$ levels are more separated, and there would be less blending between the two lines. More generally, in planning future experiments, one could gain considerably from using higher-resolution detectors, providing any sacrifice in efficiency were not too great. This would narrow the sum-energy lines with a gain in signal-to-background ratio since the background, at least in the clean region in the middle of the continuum distribution, is relatively flat.

ACKNOWLEDGMENTS

We are indebted to the staff of BESSRC for excellent technical assistance during this experiment. This work is supported by the Chemical Sciences, Geosciences, and Biosciences Division of the Office of Basic Energy Sciences, Office of Science, U.S. Department of Energy, under Contract No. W-31-109-ENG-38. P.H.M. and T.S. were supported by GSI and a NATO travel grant. Use of the Advanced Photon Source was supported by the U.S. Department of Energy, Office of Science, Basic Energy Sciences, under Contract No. W-31-109-ENG-38.

[1] M. Göppert, Naturwiss. **17**, 932 (1929).
[2] M. Göppert-Mayer, Ann. Phys. **9**, 273 (1931).
[3] B. E. J. Pagel, Nature (London) **221**, 325 (1969).
[4] L. Spitzer and J. L. Greenstein, Astrophys. J. **114**, 407 (1951).
[5] P. H. Mokler and R. W. Dunford, Phys. Scr. **69**, C1 (2004).
[6] J. Shapiro and G. Breit, Phys. Rev. **113**, 179 (1959).
[7] S. Klarsfeld, Phys. Lett. **30A**, 382 (1969).
[8] S. Klarsfeld, Lett. Nuovo Cimento **1**, 682 (1969).
[9] K. D. Bonin and T. J. McIlrath, J. Opt. Soc. Am. B **1**, 52 (1984).
[10] I. Freund, Phys. Rev. A **7**, 1849 (1973).
[11] J. Eichler, Phys. Rev. A **9**, 1762 (1974).
[12] Y.-J. Wu and J.-M. Li, J. Phys. B **21**, 1509 (1988).
[13] Y. B. Bannett and I. Freund, Phys. Rev. A **30**, 299 (1984).
[14] T. Åberg, in *Atomic Inner-Shell Processes*, edited by B. Crasemann (Academic, New York, 1975), p. 353.
[15] X.-M. Tong, J.-M. Li, L. Kissel, and R. H. Pratt, Phys. Rev. A **42**, 1442 (1990).
[16] X. Mu and B. Crasemann, Phys. Rev. A **38**, 4585 (1988).
[17] Y. Bannett and I. Freund, Phys. Rev. Lett. **49**, 539 (1982).
[18] X. Mu and B. Crasemann, Phys. Rev. Lett. **57**, 3039 (1986).
[19] D.-S. Guo, Phys. Rev. A **36**, 4267 (1987).
[20] J. H. Tung, X. M. Ye, G. J. Salamo, and F. T. Chan, Phys. Rev. A **30**, 1175 (1984).
[21] V. Florescu, Phys. Rev. A **30**, 2441 (1984).
[22] G. W. F. Drake, Nucl. Instrum. Methods Phys. Res. B **9**, 465 (1985).
[23] I. M. Savukov and W. R. Johnson, Phys. Rev. A **66**, 062507 (2002).
[24] K. Ilakovac, J. Tudorić-Ghemo, B. Bušić, and V. Horvat, Phys. Rev. Lett. **56**, 2469 (1986).
[25] K. Ilakovac, J. Tudorić-Ghemo, and S. Kaučić, Phys. Rev. A **44**, 7392 (1991).
[26] K. Ilakovac, V. Horvat, Z. Krečak, G. Jerbić-Zorc, N. Ilakovac, and T. Bokulić, Phys. Rev. A **46**, 132 (1992).
[27] P. H. Mokler and R. W. Dunford, Fiz. A **10**, 105 (2001).
[28] P. H. Mokler, H. W. Schäffer, and R. W. Dunford, Phys. Rev. A **70**, 032504 (2004).

[29] V. Florescu, S. Patrascu, and O. Stoican, Phys. Rev. A **36**, 2155 (1987).

[30] R. W. Dunford, E. P. Kanter, B. Krässig, S. H. Southworth, L. Young, P. H. Mokler, and T. Stöhlker, Phys. Rev. A **67**, 054501 (2003).

[31] In Ref. [30], the column labeled (Z=79) in Table II and the column labeled P in Table I should read, from top to bottom, 3.8(0.9), 0.32(0.5), 5.0(1), 1.6(1.4). Also, n_K should read $1.4(0.2)\times 10^{10}$ in that publication.

[32] H. W. Schäffer *et al.*, Phys. Lett. A **260**, 489 (1999).

[33] M. S. Freedman, in *Annual Review of Nuclear Science*, edited by E. Segrè (Annual Reviews, Inc., Palo Alto, 1974), Vol. 24, p. 209.

[34] M. A. Beno, C. Kurtz, A. Munkholm, U. Rütt, M. Engbretson, G. Jennings, J. Linton, G. S. Knapp, and P. A. Montano, Nucl. Instrum. Methods Phys. Res. A **A467/468**, 694 (2001).

[35] D. C. Radford, Phys. Div. Oak Ridge National Lab, URL http://radware.phy.ornl.gov/gf3.html

[36] Our ξ_j and B_ℓ differ from the ϵ_j and F parameters defined by Ilakovac *et al.* [25]. In our experiment, the solid angle was smaller so the angular correlation and the x-ray absorption could be separated.

[37] E. P. Kanter, I. Ahmad, R. W. Dunford, D. S. Gemmell, B. Krässig, S. H. Southworth, and L. Young, Phys. Rev. A **73**, 022708 (2006).

[38] The authors of Ref. [28] have indicated that the absolute value for the $3d\rightarrow 1s$ transition [lower two panels in Fig. 4 of that publication] may be too low. This line is strongly blended with the $3s\rightarrow 1s$ and $4sd\rightarrow 1s$ transitions and so the analysis has to be reconsidered. Hence, those data are not included here.

[39] H. W. Schäffer, R. W. Dunford, E. P. Kanter, S. Cheng, L. J. Curtis, A. E. Livingston, and P. H. Mokler, Phys. Rev. A **59**, 245 (1999).